Science and Technology Indonesia
e-ISSN:2580-4391 *p*-ISSN:2580-4405
Vol. 7, No. 4, October 2022

Research Paper

Synthesis and Study of Structural Properties of Calcium Oxide Nanoparticles Produced by Laser-Induced Plasma and its Effect on Antibacterial Activity

Ibrahim Karim Abbas[1]*, Kadhim Abdulwahid Aadim[1]

[1]*Department of Physics, College of Science, University of Baghdad, Baghdad, 10071, Iraq*
***Corresponding author:** Ibrahim.kareem1104a@sc.uobaghdad.edu.iq*

Abstract
A LIBS technique was used to investigate the antibacterial activity of calcium oxide nanoparticles (CaO NPs). CaO NPs were prepared using a Q-switched Nd: YAG pulsed laser with a fundamental wavelength of 1064 nm at different energies (400-600 mJ) and constant frequency (6 Hz). A calcium powder sample was prepared after being pressed into a disc with a diameter of 1 cm. Analyzing X-ray diffraction (XRD) showed the crystalline structure of CaO NPs, crystalline size was 30.99±2 and 34.20±2.2 nm for laser energy 500 and 600 mJ. (FE-SEM) to reveal the topography of produced CaO NPs, the results showed a homogenous compact and dense surface with the formation of CaO NPs like flakes, cubes, and tubes. Atomic force microscopy (AFM) has shown that the CaO NPs were nanoscale and had a coordinated surface structures. The results also revealed the stabilizing zeta potential of the prepared CaO NPs, average (ZP) -18.3±1.6 mV in 600 mJ and -8.8±2.3 mV for 500 mJ. Different laser energies used in preparing CaO NPs resulted in the varying killing of the number of bacteria *Klebsiella pneumoniae* and *Staphylococcus aureus* bacteria. Complete bacterial inhibition or cell growth inactivation was found when the laser energy prepared for the CaO NPs was 600 mJ.

Keywords
CaO NPs, CaO AFM, CaO LIP, CaO NPs FE-SEM, Zeta Potential, Laser Ablation, Bacteria

Received: 5 May 2022, Accepted: 21 August 2022
https://doi.org/10.26554/sti.2022.7.4.427-434

1. INTRODUCTION

In recent years, nanotechnology has attracted increasing interest in medical and biological research applications, to advance the area of nanomedicine (Mukherjee and Bhattacharyya, 2020). Numerous nanomaterials that improve the efficacy of delivery methods used in treating a wide range of disorders have been produced throughout the years (Nasrollahzadeh et al., 2019). Even though nanoparticles offer substantial benefits owing to their unique nanoscale features, there are still major problems in the improvement and development of nanoformulations with composites and other materials, as well as in the creation of new nanomaterials (Chin et al., 2022; Kargozar and Mozafari, 2018).

Calcium oxide nanoparticles (CaO NPs) have a wide range of medicinal and biological uses because of their non-toxicity, biocompatibility, high porosity and surface area to volume ratio (d'Amora et al., 2020). Calcium oxide nanoparticles constitute a part of the alkaline metal group, which are reactive, soft metals, calcium is the fifth most abundant element in the Earth's crust (Chen et al., 2020). Calcium exhibits a dull grey-silver appearance (Habte et al., 2019). In addition to various biological and industrial usages as an alloying agent (Habte et al., 2019; Shen et al., 2019). CaO NPs, nanodots or nanopowders are cubic or hexagonal high surface area particles (Hussein et al., 2020). Nanoscale calcium particles are typically 10–80 nm with specific surface areas in the range 30–60 m^2/g (Vergaro et al., 2015). Various nano/microparticles have been developed and optimized to increase efficacy and maintain the targeting of cancer cells among these materials.

Synthesis and showed CaO NPs are an extremely important biomaterial determined by their properties such as morphology (shape), structure (size), specific surface area, and chemical purity (Kiranda et al., 2018; Singh et al., 2018). Maleki Dizaj et al. (2019) also succeeded in synthesizing CaO NPs and indicated the possibility of using them in drug delivery because of their outstanding biocompatibility and ability to rapidly enter bacteria and cancer cells. Calcium oxide nanoparticles and microparticles are believed to be the best carriers for drug delivery. Mukherjee and Bhattacharyya (2020) have successfully explained using LIBS and the increased need for new high-productivity sterilization and disinfection technologies that are easy to implement and do not require high temperatures. This trend has taken on a significant amount of significance in recent years. As a result of their distinct features from their bulk

equivalents, nanomaterials have attracted a significant deal of attention in recent years (Nasrollahzadeh et al., 2019).

Nanomaterials, which are incredibly small in size and have a large surface area, have demonstrated significant biological activity in the human body (Contera et al., 2020). Essential in biomedicine (Ciofani, 2018). In spite of this, our present understanding of the behavior of nanomaterials with human health is still insufficient (Abedin et al., 2021). The growth of nanotechnology for biomedical applications necessitates the development of a chemical-free production technique (Chin et al., 2022). As well as having the potential to change health, nanotechnology has already posed significant regulatory issues for the scientific communities working in nanomedicine (Kabir et al., 2018). Materials with unique qualities at the nanoscale can address critical medical demands; these materials are already being utilized as the base for a novel therapy or medicine for biological and other applications (Nikaeen et al., 2020).

For this reason, so, we synthesized CaO NPs by laser-induced plasma at multi-laser energy and pulses and employed CaO NPs by LIP to increase the killing impact on oral bacteria (*Staphylococcus aureus* and *Klebsiella pneumoniae*) isolated from the teeth. The combined laser-induced plasma and CaO NPs treatment, on the other hand, produced severe bacteria cell damage, resulting in the loss of intracellular components from many bacterial cells and the death of bacteria (Ahmadian et al., 2018).

2. EXPERIMENTAL SECTION

2.1 Laser-Induced Plasma System Setup

An Nd-YAG laser with a fundamental wavelength of 1064 nm and at varying energies (400–600 mJ) at 6 Hz was used in the study. Calcium powder with a purity content of 99.99%, purchased from (E. MERCK, D-6100 Darmstadt, Manufactured in Germany). A calcium sample was placed 10 cm away from the laser head to expose it to bombardment and prepare calcium oxide nanoparticles. The angle of the bombing operation of the calcium sample was 90° vertically. The experiment was performed at normal atmospheric pressure. Figure 1 shows the laser-induced plasma system with the calcium sample target.

2.2 CaO NPs Preparation

A pressure of 10 tons was applied on a 2 g sample of pure micro-calcium powder using a hydraulic press. The calcium sample was prepared and compressed under 8 tons of pressure for 15 min. The sample used for laser bombardment was circular with a diameter of 1 cm. Where the calcium sample was placed in a 10 mL beaker with distilled water at a distance of 10 cm from the aperture of the laser system, then laser bombardment of the calcium sample was performed at different number pulses (100–300) of the used energies (400–600 mJ). During the bombardment, the molecules from the laser-induced plasma interact with the liquid inside the beaker, producing a series of reactions with the calcium surface and leading to a change in the color of the liquid and resulting in calcium oxide nanoparticles with characteristics that depend on the different energies used to prepare nanoparticles. The characterization of the produced CaO NPs nanoparticles was carried out in Iran at the University of Kashan for XRD (XPERT PAANALTICAL PHILLIPS HOLLAND), FE-SEM, EDS (TESCN MIRA3 FRENCH), and TEM, with Zeta Potential (HORBIA Scientific SZ-100 Poland).

2.3 Types of Bacteria Used

Two strains of bacteria used in the study, gram-negative *Klebsiella pneumoniae* and gram-positive *Staphylococcus aureus*, were obtained from the Central Environmental Laboratory at the University of Baghdad-College of Science. Nutritional broths were prepared by dissolving 37 g of powder in 1 liter of distilled water. For bacteria growth, we used, which is Mueller Hinton Agar, both types of bacteria isolated then identified by biochemical test and Vitek system from clinical blaque tooth and prepared with the nutritional broth Mueller Hinton Agar.

2.4 Inoculum Preparation and CaO NPs Exposure

Two strains of bacteria, *Klebsiella pneumoniae* and *Staphylococcus aureus*, were cultured on nutritional broth for 24 hours at 37°C to prepare the inoculum. The samples were suspended overnight in sterile water to prepare the final inoculum concentration that contains CaO NPs. The quantity of the bacterial cell was expressed in terms of colony-forming units (CFU). The initial cell concentrations of *S. aureus* and *K. pneumoniae* bacteria were 9×10^{10} and 9.9×10^{10} CFU/mL, respectively. The laser-induced plasma system generated CaO NPs, which were then carefully swabbed on the bacteria on a petri dish. After that, we added 0.1 mL of CaO NPs to a petri dish containing bacteria grown in a nutrient broth overnight. The treated dishes were then incubated for 24 h at 37°C. The extent of inhibitory or killing activity was then determined for all the treated dishes. This method was used to evaluate the response of both types of bacteria to CaO NPs (Mohamed et al., 2017).

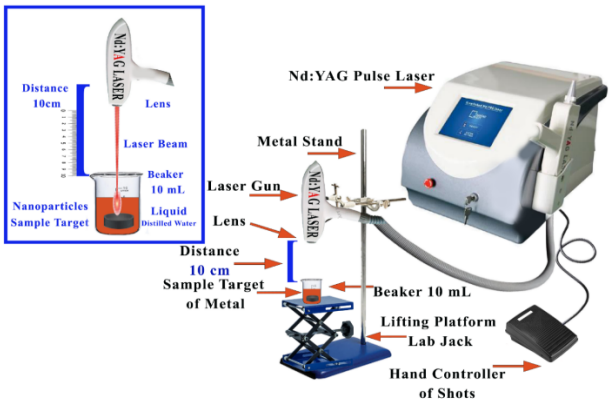

Figure 1. Schematic the of Laser-Induced Plasma Setup for Preparing Calcium Oxide Nanoparticles

3. RESULT AND DISCUSSION

3.1 Investigation of the Crystal Structure

It is shown in Figure 2 that the CaO NPs X-ray diffraction (XRD) pattern had an angular range of 30° to 80°. The spectrum of calcium oxide nanoparticles produced by laser-induced plasma at 500 and 600 mJ for 300 shots fits the crystalline structure of CaO the reference card no. (82-1691) with the appearance of several different peaks at 500 and 600 mJ, which were observed at 2θ°= (34.38°) (38.02°) (54.83°) (65.13°) (67.59°), the clear figure of the XRD spectrum indicates that the intensity of the peaks at laser energy 600 mJ is slightly higher than the intensity of the peaks at 500 mJ preparing the CaO nanoparticles, and these results are consistent with the results of EDX spectrum analysis. Whereas the increase in the laser energy and the interaction of laser pulses with the calcium sample in the beaker had an effect on the size of the prepared CaO nanoparticles. The crystal size of the synthesized CaO nanoparticles was calculated from the Debye–Scherer equation (Preetham et al., 2016):

$$D(A^{\circ}) = \frac{k\lambda}{\beta \cos\theta}$$

Where in this equation formula, D crystal size, β: full width at half maximum of the peak (FWHM), λ represent X-ray wavelength (1.54 Å), k is the shape factor which is always close to unity (0.9). As it the apparent peaks in the figure also confirms its agreement with the research and literature published by other researchers to prepare calcium oxide nanoparticles (Preetham et al., 2016), where the crystallite size of the prepared nanoparticles is estimated to be about 30.991±2 nm at 600 mJ and 34.202±2.2 nm at 500 mJ. Clearly, from Figures 2A and 2B, the highest peak was at 38.02° for the laser energies 500 and 600 mJ, while the lowest peak was at the angle of 67.59°, where the anisotropy increases with an increase in particle size. In addition, the presence of stacking errors may reduce a coherent scattering area along the direction or at the top (38.02°) compared to other directions (Anantharaman et al., 2016).

3.2 Atomic Force Microscopy of Calcium Oxide Nanoparticles

Calcium nanorods with an average diameter of 46.56 nm, an average particle size of 22.19 nm, and roughness of 11.38 nm were formed at 500 mJ. Some spherical calcium nanoparticles were observed, as depicted in Figure 3 and Figure 4. The particle size distribution of CaO NPs ranged from 55 to 125 nm with a mean value of 49.87 nm, as shown in Figure 3. At 600 mJ, the CaO NPs had an average diameter of 30.62 nm, an average particle size of 14.76 nm, a roughness of 7.518 nm, and a mean value of particle size of 41.09 nm from the distribution plot, as shown in Figure 4. The formation of calcium nanoparticles at an energy of 600 mJ is similar to the layer-by-layer formation and appears more interconnected and

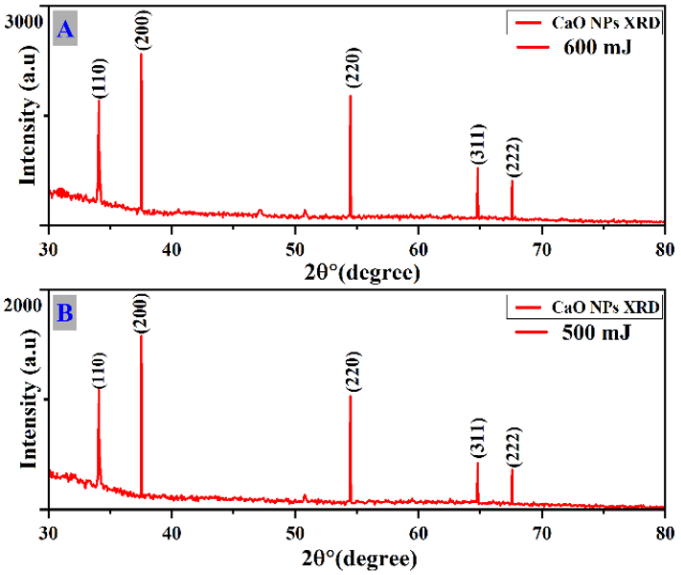

Figure 2. XRD Patterns of Calcium Nanoparticles Prepared by Laser-Induced Plasma at A) 600 and B) 500 mJ

uniform. The interaction occurs extremely quickly when the laser beam exiting the lens comes in contact with the calcium sample in the beaker, resulting in clusters of uniform size and symmetry, this compatible with (Bala et al., 2017).

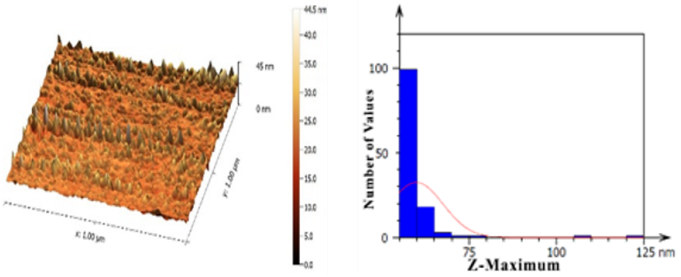

Figure 3. 3D Topography Surface Image AFM and Histogram Distribution of Calcium Oxide Nanoparticles Prepared by Laser-Induced Plasma at Laser Energy 500 mJ

3.3 Scanning Electron Microscopy (SEM) Analysis of CaO NPs

The surface morphology of calcium oxide nanoparticles prepared by laser-induced plasma at 500 and 600 mJ are shown in Figures 5 and 6, respectively. Energy-dispersive X-ray spectroscopy (EDX) was also performed to determine the concentration of elements in a solution of calcium oxide nanoparticles, which confirmed the formation of CaO. Analyzing the chemical composition of produced CaO samples was done using the EDX technique. The EDX spectrum shows that the nanoparticles include peaks associated with Ca and O elements. There were no additional impurities in the nanoparticles, as confirmed by the EDX examination.

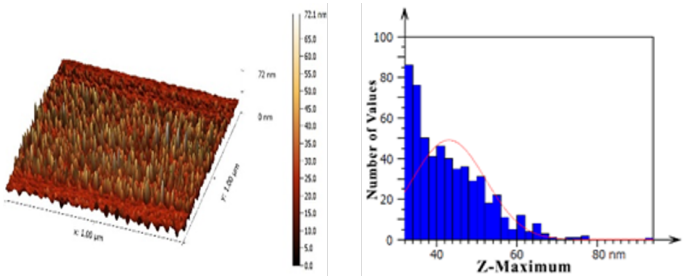

Figure 4. 3D Topography Surface Image AFM and Histogram Distribution of Calcium Oxide Nanoparticles Prepared by Laser-Induced Plasma at Laser Energy 600 mJ

The EDX spectra show that the LIBS approach synthesis CaO nanoparticles. The results reveal that raising the laser energy produced exceedingly small particles, agreeing with previous research (Hussein et al., 2020). Two lasers (500 and 600) mJ were employed to record percentages of the Ca and O components as shown in Figure 7. In the FE-SEM of calcium oxide nanoparticles, the photos depict the magnification that was used showed morphology and uniform surface area. We can see from the images and zoom view that the results in forming nanostructure of calcium oxide particles for used energies. The image shows a variety of shapes of synthesized calcium oxide nanoparticles with several spaces between the nanoparticles, which become denser when the laser energy used increases from 500 to 600 mJ. These nanoparticles were characterized by tubes with diameters in the nanoscale that formed grids connected like flakes, cubes, tubes, and flowers. The calcium oxide nanoparticles exhibited a uniform distribution, as shown in Figures 5 and 6.

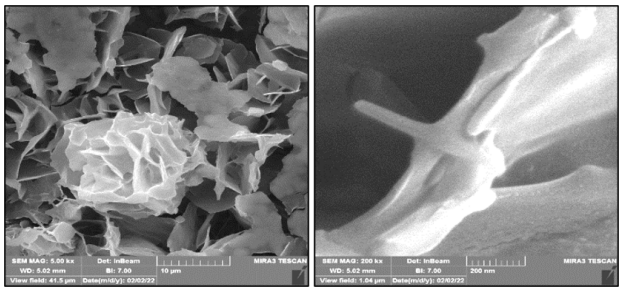

Figure 5. FE-SEM Microstructure Morphology Images of Calcium Oxide Nanoparticles at Magnification Scale (10 μm+200 nm) Prepared by Laser-Induced Plasma at Laser Energy 500 mJ

3.4 Zeta Potential (ZP) of CaO NPs

When the dispersion medium and stationary fluid layer are coupled to a dispersed particle, the zeta potential is the difference in potential between the two media. The stability of colloidal dispersions is indicated by the value of the zeta potential. Electrostatic stabilization is achieved in colloids with high

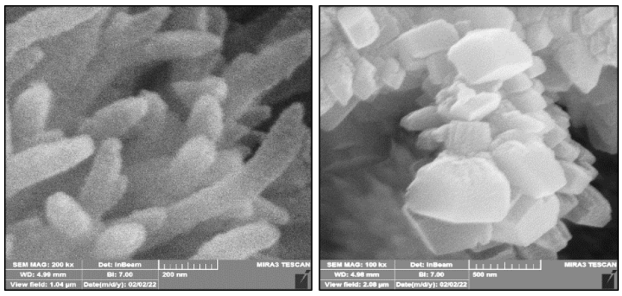

Figure 6. FE-SEM Microstructure Morphology Images of Calcium Oxide Nanoparticles at Magnification Scale (10 μm+200 nm) Prepared by Laser-Induced Plasma at Laser Energy 600 mJ

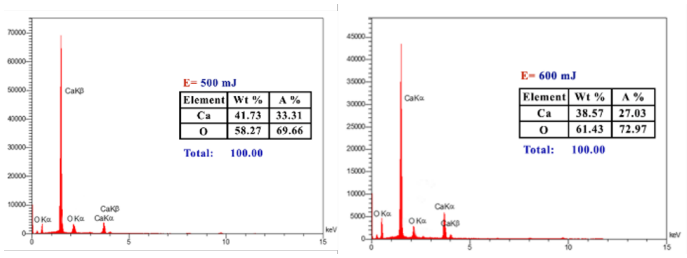

Figure 7. EDX Spectrum of Calcium Oxide Nanoparticles Prepared at Laser Energies 500 and 600 mJ

zeta potential (negative or positive), whereas coagulation and flocculation are achieved in colloids with low zeta potentials (Clogston and Patri, 2011).

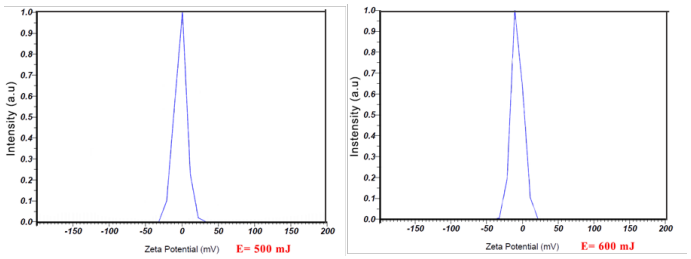

Figure 8. Zeta Potential of Calcium Oxide Nanoparticles Prepared by Laser Induced Plasma at 500 and 600 mJ

Figure 8 shows the zeta-potential of calcium oxide nanoparticles prepared by laser-induced plasma at 500 and 600 mJ. Where the average measurements of zeta potential (ZP) value -8.8±2.3 mV at laser energy 500 mJ, whereas average zeta potential -18.3±1.6 mV at 600 mJ, indicate they have a high degree of stability, the high values of ZP mean that the synthesized CaO NPs are highly charged particles and in turns will prevent the aggregation and agglomeration via their large repulsion force. At first laser energy, 500 mJ calcium oxide nanoparticles with ZP of -8.8±2.3 mV indicate that they have low dispersion, which leads to some particles aggregation and or agglomeration, coagulation, or flocculation due to Van der

Waals attraction force, whereas CaO NPs at laser energy 600 mJ have ZP -18.3±1.6 mV considered better colloidal stability condition. Nanoparticles agglomerate due to their high free surface energy and huge surface area.

3.5 CaO NPs Cell Growth Inactivation of *S. aureus* and *K. pneumoniae*

Figure 9 shows the *Staphylococcus aureus* and *Klebsiella pneumoniae* after being cultured on a petri dish in nutrient media for 24 hours before exposing both types of bacteria to CaO NPs. The effects of CaO NPs differed based on the type of bacteria used, as well as the laser energy used in the creation of the CaO and the laboratory conditions. According to NPs results, different laser energies inhibited bacteria cells in different laser shots, indicating that the quantity of CaO NPs created as well as the size of the nanoparticles is a significant influence on the inhibition rates for both types of bacteria. The calcium ions dissolved in the distilled water during the preparation of nanoparticles had a significant effect and were responsible for inhibiting bacteria during nanoparticle preparation using different laser energies.

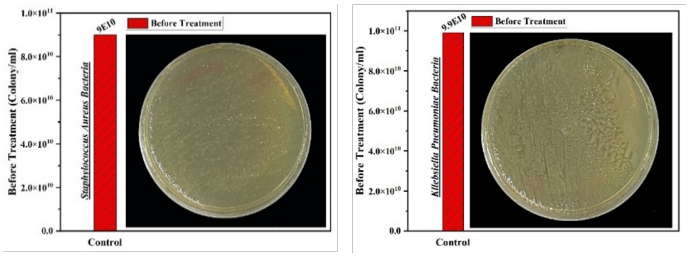

Figure 9. *Staphylococcus aureus* and *Klebsiella pneumoniae* Bacteria Before CaO NPs Treatment

It is expected that the positively charged surface of gram-negative bacteria, which is at near neutral pH due to the presence of lipopolysaccharides, will interact with the negatively charged surface of nanoparticles, resulting in the suppression of enzyme synthesis in the bacteria (Singh et al., 2021). Metal oxide nanoparticles induce ROS production in bacteria (Rambabu et al., 2021). Evidence suggests that metal ions produced by nanoparticles interfere with and block enzymes in the respiratory chain (Gur et al., 2022). As a result of this process, singlet oxygen, hydroxyl radicals, hydrogen peroxide, superoxide anions, and other ROS are generated and stored. The interaction of nanoparticles with bacterial cells causes cell membrane leakage, induces oxidative stress, and ultimately leads to cell death.

CaO NPs prepared at 400, 500 and 600 mJ, and the concentration of solutions of CaO NPs was proportional directly to the number of pulses. Where at 400 mJ with different pulses (100, 200 and 300), the concentration of the prepared CaO NPs was 33, 47.4 and 64.3 mg/L respectively, and at 500 mJ for the same pulses was 49.6, 71.2 and 84.75 mg/L respectively, also at 600 mJ the concentration 55.8, 79.7 and 94 mg/L for the same pulses. Therefore, 100 shots resulted in the least concentration and least effective bacterial activity in all laser energies. The three different shots were used for each type of bacteria. The gram-positive bacteria, *Staphylococcus aureus*, showed a stronger cohesion in their cell wall than the gram-negative bacteria *Klebsiella pneumoniae*, as shown in Figure 10. In *Staphylococcus aureus* bacteria, at the laser energy of 400 mJ the number of the colony was 5.1×10^{10} and 1.3×10^{10} Colony/mL at the concentration of 33 and 47.4 mg/L for a number of pulses (100-200) respectively, and at 300 pulse we get perfect killing at the same energy 400 mJ. Also, at 500 mJ the number of the colony was 4.4×10^{10} and 1.8×10^{10} Colony/mL at the concentration of 49.6 and 71.2 mg/L for the number of pulses (100-200) respectively, and at 300 pulses we also get perfect killing. As well, at laser energy 600 mJ for different laser shots we get on perfect killing for *Staphylococcus aureus* bacteria.

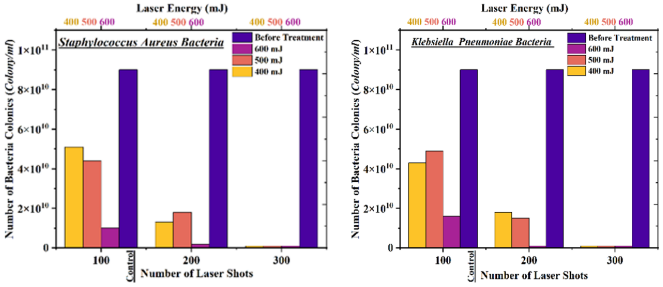

Figure 10. Illustrated the Number of Bacteria Colonies Plots of *S. aureus* and *K. pneumoniae* Bacteria Before and After Treatment by CaO NPs prepared at Different Laser Energies (400-600 mJ) and Varying Laser Pulses (100-300)

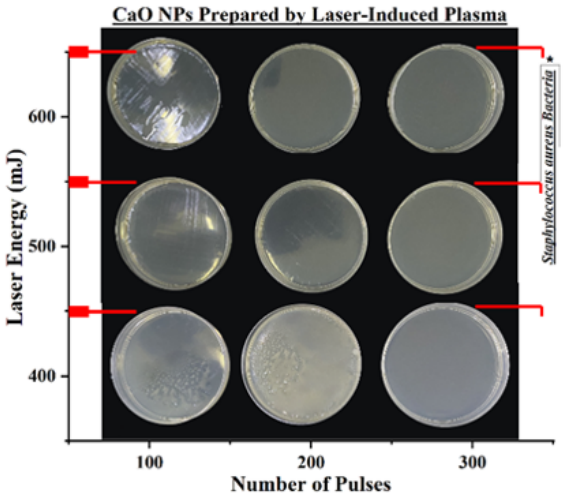

Figure 11. *Staphylococcus aureus* Bacteria After Treatment by CaO NPs at Different Laser Energies (400-600 mJ) and Laser Pulses (100-300)

In the first concentration 33 mg/L at 400 mJ and 100 pulses, the CaO NPs did not reach higher concentrations. Therefore,

the number of calcium ions emitted from the sample in the solution was very low, and the same was true for the second concentration of 47.4 mg/L for 200 pulses, the concentration of CaO NPs in the solution increased to increase the laser energy and the number of shots, so the number of emitted and interacting ions was more than in the first time, and at the last 300 pulses, the concentration of CaO NPs increased, so the result of the effectiveness and impact of these particles was higher than in the previous two cases. At 500 mJ, the concentration of nanoparticles increased from that of 400 mJ for all numbers of shots because of increased laser energy. Thus at 100 pulses at 500 mJ, the concentration of CaO NPs was 49.6 mg/L, higher than that at 400 mJ for the same number of pulses, increasing the effectiveness of the nanoparticles in killing bacteria. Because an increased inhibition with increased laser energy, we may conclude that calcium oxide nanoparticles in laser-induced plasma systems work best when exposed to diverse laser energies at different pulses. Toxic effects are mostly induced by direct contact between calcium oxide nanoparticles and the cell wall of the bacteria; therefore, the cell wall plays a key role in preventing cell rupture and the subsequent exocytosis of cell components that leads to bacterial death. These results agree with prior researchers (Gudkov et al., 2021).

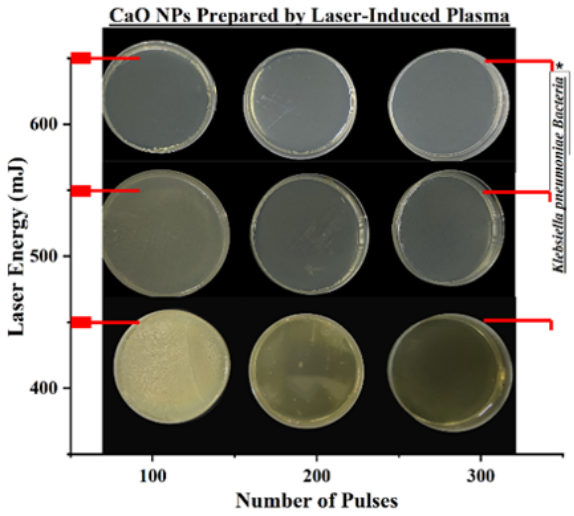

Figure 12. *Klebsiella pneumoniae* Bacteria After CaO NPs Treatment at Different Laser Energies (400-600 mJ) and Laser Pulses (100-300)

Figure 10 indicates that for *Klebsiella pneumoniae* bacteria, the numbers of colonies were 4.3×10^{10} and 1.8×10^{10} colonies/mL when the CaO NPs concentrations were 33 (100 pulse) and 47.4 mg/L (200 pulse), respectively, at 400 mJ. All the bacteria were killed when the CaO NPs were prepared at 300. At 500 mJ, the numbers of colonies were 4.9×10^{10} and 1.5×10^{10} colonies/mL when the CaO NPs concentrations were 49.6 (100 pulse) and 71.2 mg/L (200 pulse), respectively. Similar to the CaO NPs prepared at 400 mJ, all the bacteria were killed when the CaO NPs were prepared at 300 pulse at 500 mJ. At 600 mJ, all the *Klebsiella pneumoniae* bacteria were killed, regardless of the shots. The cell wall in this bacteria is less resistant than that of gram-positive bacteria, as shown in Figure 11; the percentage of bacterial inhibition or cell growth inactivation increased when the laser energy for preparing CaO NPs increased. The cell wall of *Klebsiella pneumoniae* bacteria offered less impedance to the positive cell wall, which is in agreement with previous literature (Gur et al., 2022; Wang et al., 2022).

In gram-positive bacteria, the cell walls are coated with thick peptidoglycan, but in gram-negative bacteria, an additional outer membrane of lipopolysaccharides is present. Carbohydrates (cellulose) and proteins create a multi-sheath stiff complex that makes up the cell wall (Ru et al., 2019). In *Klebsiella pneumoniae* bacteria, the peptidoglycan layer is much thinner than in *Staphylococcus aureus*. Due to the lack of the thick peptidoglycan layer in gram-positive *Klebsiella pneumoniae* bacteria, they are more susceptible to cell wall disintegration when CaO NPs interact with the cell wall. Gram-negative *Klebsiella pneumoniae* bacteria may also be vulnerable to nanoparticles because they are coated with lipopolysaccharide molecules with a negative charge, as shown in Figure 12. The results are in agreement with (Li et al., 2014).

4. CONCLUSION

Calcium oxide nanoparticles (CaO NPs) were synthesized by laser-induced plasma at different laser energies (400-600 mJ) and pulses (100-300). The XRD pattern showed crystalline structure and several peaks from CaO NPs at (500-600 mJ); the results showed a crystalline size of 30.99 nm in 600 mJ whereas crystalline size was 34.20 nm in 500 mJ. EDX revealed the presence of calcium and oxygen at different percentages in 500 and 600 mJ. FE-SEM images revealed the morphology of nanoparticles and agglomeration of CaO NPs, including in the form of tubes and flakes, where the average diameter was 46.56 and 30.62 nm for 500 and 600 mJ, respectively. As clearly nanoscale and had a coordinated surface structures as in AFM images. In addition, a degree of stability of average zeta potential-18.3±1.6 mV in 600 mJ and -8.8±2.3 mV for 500 mJ for laser energy. Two types of bacteria were exposed to CaO NPs, and a different killing number of bacteria colonies at laser energies (400-500) mJ with complete bacteria killing were obtained at laser energy 600 mJ for all laser pulses.

5. ACKNOWLEDGMENT

We would like to express gratitude and grateful thanks and deeply extend thanks to the plasma laboratory in physics department-college of sciences/Baghdad University. And finally, we offer gratitude to everyone who gave us the inspiration to continue the thorough knowledge path.

REFERENCES

Abedin, F., E. Asmatulu, and M. N. Andalib (2021). Nanomaterials and Human Health: an Overview. *Nanotoxicology and*

Nanoecotoxicology, **2**; 165–180
Ahmadian, E., S. Shahi, J. Yazdani, S. M. Dizaj, and S. Sharifi (2018). Local Treatment of the Dental Caries Using Nanomaterials. *Biomedicine & Pharmacotherapy*, **108**; 443–447
Anantharaman, A., S. Ramalakshmi, and M. George (2016). Green Synthesis of Calcium Oxide Nanoparticles and its Applications. *International Journal of Engineering Research and Application*, **6**(10); 27–31
Bala, W. A., V. Benitha, K. Jeyasubramanian, G. Hikku, P. Sankar, and S. V. Kumar (2017). Investigation of Anti-Bacterial Activity and Cytotoxicity of Calcium Fluoride Nanoparticles. *Journal of Fluorine Chemistry*, **193**; 38–44
Chen, P., Y. Wang, S. He, P. Wang, Y. Xu, and L. Zhang (2020). Green Synthesis of Spherical Calcium Hydroxide Nanoparticles in the Presence of Tannic Acid. *Advances in Materials Science and Engineering*, **2020**
Chin, B. L., F. H. Juwono, and K. S. Yong (2022). Nanotechnology and Nanomaterials for Medical Applications. In *Nanotechnology for Electronic Applications*. Springer; 63–87
Ciofani, G. (2018). *Smart Nanoparticles for Biomedicine*. Elsevier
Clogston, J. D. and A. K. Patri (2011). Zeta Potential Measurement. *Characterization of Nanoparticles Intended for Drug Delivery*. Springer; 63–70
Contera, S., J. Bernardino de la Serna, and T. D. Tetley (2020). Biotechnology, Nanotechnology and Medicine. *Emerging Topics in Life Sciences*, **4**(6); 551–554
d'Amora, M., F. Liendo, F. A. Deorsola, S. Bensaid, and S. Giordani (2020). Toxicological Profile of Calcium Carbonate Nanoparticles for Industrial Applications. *Colloids and Surfaces B: Biointerfaces*, **190**; 110947
Gudkov, S. V., D. E. Burmistrov, D. A. Serov, M. B. Rebezov, A. A. Semenova, and A. B. Lisitsyn (2021). A Mini Review of Antibacterial Properties of ZnO Nanoparticles. *Frontiers in Physics*, **9**; 641481
Gur, T., I. Meydan, H. Seckin, M. Bekmezci, and F. Sen (2022). Green Synthesis, Characterization and Bioactivity of Biogenic Zinc Oxide Nanoparticles. *Environmental Research*, **204**; 111897
Habte, L., N. Shiferaw, D. Mulatu, T. Thenepalli, R. Chilakala, and J. W. Ahn (2019). Synthesis of Nano-Calcium Oxide from Waste Eggshell by Sol-Gel Method. *Sustainability*, **11**(11); 3196
Hussein, A. I., Z. Ab-Ghani, A. N. Che Mat, N. A. Ab Ghani, A. Husein, and I. Ab. Rahman (2020). Synthesis and Characterization of Spherical Calcium Carbonate Nanoparticles Derived from Cockle Shells. *Applied Sciences*, **10**(20); 7170
Kabir, E., V. Kumar, K. H. Kim, A. C. Yip, and J. Sohn (2018). Environmental Impacts of Nanomaterials. *Journal of Environmental Management*, **225**; 261–271
Kargozar, S. and M. Mozafari (2018). Nanotechnology and Nanomedicine: Start Small, Think Big. *Materials Today: Proceedings*, **5**(7); 15492–15500
Kiranda, H. K., R. Mahmud, D. Abubakar, and Z. A. Zakaria (2018). Fabrication, Characterization and Cytotoxicity of Spherical-Shaped Conjugated Gold-Cockle Shell Derived Calcium Carbonate Nanoparticles for Biomedical Applications. *Nanoscale Research Letters*, **13**(1); 1–10
Li, B., Y. Zhao, C. Liu, Z. Chen, and D. Zhou (2014). Molecular Pathogenesis of *Klebsiella pneumoniae*. *Future Microbiology*, **9**(9); 1071–1081
Maleki Dizaj, S., S. Sharifi, E. Ahmadian, A. Eftekhari, K. Adibkia, and F. Lotfipour (2019). An Update on Calcium Carbonate Nanoparticles as Cancer Drug/Gene Delivery System. *Expert Opinion on Drug Delivery*, **16**(4); 331–345
Mohamed, M. M., S. A. Fouad, H. A. Elshoky, G. M. Mohammed, and T. A. Salaheldin (2017). Antibacterial Effect of Gold Nanoparticles Against *Corynebacterium pseudotuberculosis*. *International Journal of Veterinary Science and Medicine*, **5**(1); 23–29
Mukherjee, A. and S. Bhattacharyya (2020). Nanotechnology in Medicine. *Biotechnology Business-Concept to Delivery*. Springer; 57–64
Nasrollahzadeh, M., S. M. Sajadi, M. Sajjadi, and Z. Issaabadi (2019). An Introduction to Nanotechnology. In *Interface Science and Technology*, **28**; 1–27
Nikaeen, G., S. Abbaszadeh, and S. Yousefinejad (2020). Application of Nanomaterials in Treatment, Anti-Infection and Detection of Coronaviruses. *Nanomedicine*, **15**(15); 1501–1512
Preetham, H. S., G. M. Madhu, B. Brijesh, and K. V. K. Pai (2016). High Temperature CO_2 Sorption Using $Ca(OH)_2$ in Pilot Scale Packed Column. *European Journal of Chemistry*, **7**(2); 176–181
Rambabu, K., G. Bharath, F. Banat, and P. L. Show (2021). Green Synthesis of Zinc Oxide Nanoparticles Using *Phoenix dactylifera* Waste as Bioreductant for Effective Dye Degradation and Antibacterial Performance in Wastewater Treatment. *Journal of Hazardous Materials*, **402**; 123560
Ru, X., Y. Guo, Z. Bai, X. Xie, X. Ma, L. Zhu, K. Wang, F. Wang, L. Yang, and J. Lu (2019). Synthesis of Calcium Carbonate Nanoparticles in Erythrocytes Enables Efficient Removal of Extracellular Lead Ions. *Communications Chemistry*, **2**(1); 1–7
Shen, C., R. Li, J. Pei, J. Cai, T. Liu, and Y. Li (2019). Preparation and the Effect of Surface-Functionalized Calcium Carbonate Nanoparticles on Asphalt Binder. *Applied Sciences*, **10**(1); 91
Singh, J. P., W. C. Lim, S. O. Won, J. Song, and K. H. Chae (2018). Synthesis and Characterization of Some Alkaline-Earth-Oxide Nanoparticles. *Journal of the Korean Physical Society*, **72**(8); 890–899
Singh, T. A., A. Sharma, N. Tejwan, N. Ghosh, J. Das, and P. C. Sil (2021). A State of the Art Review on the Synthesis, Antibacterial, Antioxidant, Antidiabetic and Tissue Regeneration Activities of Zinc Oxide Nanoparticles. *Advances in Colloid and Interface Science*, **295**; 102495
Vergaro, V., E. Carata, E. Panzarini, F. Baldassare, L. Dini, and G. Ciccarella (2015). Synthesis of Calcium Carbonate Nanocrystals and Their Potential Application as Vessels for Drug Delivery. *AIP Conference Proceedings*, **1667**; 020014

Wang, L. L., C. Yang, and S. Liu (2022). Development and Antibacterial Activity of Zinc Oxide Nanoparticles Encapsulated in Core–Shell Microparticles for Managing Enterotoxigenic *Escherichia coli*-Related Post-Weaning Diarrhea. *Applied Nanoscience*, **12**(5); 1449–1458

